AGU PUBLICATIONS

JGR

Journal of Geophysical Research: Oceans

RESEARCH ARTICLE

10.1002/2015JC011093

Key Points:
- Evaporation of oil is modeled using comprehensive composition derived from GC-VUV-MS analysis
- Modeled surface slick compositions suggest significant subsurface transport of oil during the DWH disaster
- Oil evaporation, particularly intermediate volatility compounds leads to significant secondary organic aerosol

Supporting Information:
- Supporting Information S1

Correspondence to:
G. T. Drozd,
ahg@berkeley.edu,
drozd@berkeley.edu

Citation:
Drozd, G. T., D. R. Worton, C. Aeppli, C. M. Reddy, H. Zhang, E. Variano, and A. H. Goldstein (2015), Modeling comprehensive chemical composition of weathered oil following a marine spill to predict ozone and potential secondary aerosol formation and constrain transport pathways, *J. Geophys. Res. Oceans*, *120*, 7300–7315, doi:10.1002/2015JC011093.

Received 30 JUN 2015
Accepted 12 OCT 2015
Accepted article online 15 OCT 2015
Published online 9 NOV 2015

Modeling comprehensive chemical composition of weathered oil following a marine spill to predict ozone and potential secondary aerosol formation and constrain transport pathways

Greg T. Drozd[1], David R. Worton[2], Christoph Aeppli[3], Christopher M. Reddy[4], Haofei Zhang[1], Evan Variano[5], and Allen H. Goldstein[1]

[1]Department of Environmental Science, Policy and Management, University of California, Berkeley, California, USA, [2]National Physical Laboratory, Middlesex, UK, [3]Bigelow Laboratory for Ocean Sciences, East Boothbay, Maine, USA, [4]Department of Marine Chemistry and Geochemistry, Woods Hole Oceanographic Institution, Woods Hole, Massachusetts, USA, [5]Department of Civil and Environmental Engineering, University of California, Berkeley, California, USA

Abstract Releases of hydrocarbons from oil spills have large environmental impacts in both the ocean and atmosphere. Oil evaporation is not simply a mechanism of mass loss from the ocean, as it also causes production of atmospheric pollutants. Monitoring atmospheric emissions from oil spills must include a broad range of volatile organic compounds (VOC), including intermediate-volatile and semivolatile compounds (IVOC, SVOC), which cause secondary organic aerosol (SOA) and ozone production. The Deepwater Horizon (DWH) disaster in the northern Gulf of Mexico during Spring/Summer of 2010 presented a unique opportunity to observe SOA production due to an oil spill. To better understand these observations, we conducted measurements and modeled oil evaporation utilizing unprecedented comprehensive composition measurements, achieved by gas chromatography with vacuum ultraviolet time of flight mass spectrometry (GC-VUV-HR-ToFMS). All hydrocarbons with 10–30 carbons were classified by degree of branching, number of cyclic rings, aromaticity, and molecular weight; these hydrocarbons comprise ~70% of total oil mass. Such detailed and comprehensive characterization of DWH oil allowed bottom-up estimates of oil evaporation kinetics. We developed an evaporative model, using solely our composition measurements and thermodynamic data, that is in excellent agreement with published mass evaporation rates and our wind-tunnel measurements. Using this model, we determine surface slick samples are composed of oil with a distribution of evaporative ages and identify and characterize probable subsurface transport of oil.

1. Introduction

The explosion and sinking of the *Deepwater Horizon* (DWH) oil rig on 20 April 2010 released approximately five million barrels of Mississippi Canyon sweet, light crude oil (*MC-252*) into the Gulf of Mexico [*McNutt et al.*, 2011; *Reddy et al.*, 2012]. In addition to the massive amounts of persistent components of the oil that remained at various depths in the water column and oiled shorelines, the more volatile, nonsoluble oil components were released to the atmosphere. Evaporation was estimated to account for the loss of 5–20% of spilled oil mass, with cleanup interventions (e.g., skimming and burning), dissolution, biodegradation, photooxidation, and dispersion accounting for the majority of the remaining loss [*The Federal Interagency Solutions Group, Oil Budget Calculator Science and Engineering Team*, 2013; *Ryerson et al.*, 2012]. NOAA aircraft measurements during the DWH spill clearly demonstrated the ability of oil spill emissions to severely impact air quality at the airshed spatial scale, with some pollutants in the marine atmosphere reaching levels considered high even for urban areas [*de Gouw et al.*, 2011; *Middlebrook et al.*, 2011; *Ryerson et al.*, 2011; *Yuan et al.*, 2014]. A significant plume of organic aerosol was detected downwind of the DWH site [*Middlebrook et al.*, 2011], and composition measurements indicated its source as evaporated oil that was then oxidized in the atmosphere to form secondary organic aerosol (SOA) [*de Gouw et al.*, 2011; *Middlebrook et al.*, 2011]. This showed SOA production from spilled oil can occur over a large area at levels that may be significant compared to ambient air quality standards (up to 20 $\mu g/m^3$) [*de Gouw et al.*, 2011; *Middlebrook et al.*, 2011]. Ship activity, flaring of released gases, and burning of spilled oil also led to elevated NO_x and ozone levels in the vicinity of the spill [*Middlebrook et al.*, 2011]. Pollutant formation could have been even more pronounced, except that the oil was released from 1500 m below the surface and small aromatics and aliphatics were lost in significant amounts to dissolution in the water

column [*Ryerson et al.*, 2011]. In addition, the oxidation of oil vapors, which leads to formation of SOA, continues over the course of several days [*Jimenez et al.*, 2009], broadening the area and time scale impacted by release of oil vapors to the atmosphere. For this reason, the effects of emissions may be dramatic further from the spill site than expected, and this was indeed the case with the DWH spill as reported in organic aerosol measurements by *Middlebrook et al.* [2011]. The DWH spill thus made clear the importance of predicting and measuring atmospheric effects of oil spills beyond simply mass loss of oil from the ocean.

Weathering, or aging, of spilled oil results from a range of physical processes (evaporation, dissolution, emulsification, etc.) and chemical processes (photooxidation, biodegradation), and causes significant changes in oil composition (e.g., average molecular weight) and properties (e.g., viscosity). In addition to the complexity of numerous weathering processes, oil is itself extremely complex, making accurate description and prediction of the effects of weathering quite difficult. Oil extraction by deep-sea rigs, such as the DWH, and application of dispersants present even more difficulties in terms of understanding weathering and the fate of oil because of subsurface oil transport and weathering [*Socolofsky et al.*, 2011]. Information on oil composition and prediction of time-resolved weathering effects is crucial in spill response measures for several reasons including: determining window of opportunity for response measures (burning, dispersant application), formulation of dispersants, and predicting interactions of weathered oil with marine snow leading to flocculation events [*Passow*, 2014; *Chanton et al.*, 2015; *Valentine et al.*, 2014]. The effects mentioned above on air quality and human health from atmospheric emissions of oil spills are most directly related to evaporative weathering, but all weathering and transport processes are coupled.

Extensive work has been done to determine effective metrics of oil weathering (ratios of select saturates to aromatics, etc.), and laboratory simulation of weathering has led to significant gains in understanding of the effects of weathering, but comprehensive prediction of the temporal evolution of oil composition has generally not been feasible [*Gros et al.*, 2014; *Stiver and Mackay*, 1984; *Daling et al.*, 2014]. In this work, we utilize advances in gas chromatography and mass spectrometry analysis to yield nearly complete composition of extremely complex mixtures like crude oil. Gas chromatography with vacuum ultraviolet high-resolution time-of-flight mass spectrometry (GC-VUV-HR-ToFMS) was used to characterize all hydrocarbons of weathered *MC-252* oil with between 10 and 30 carbons according to degree of branching, number of cyclic rings, aromatic character, and molecular weight. This technique involves boiling-point separation followed by ionization with minimal fragmentation and high-resolution mass selective detection. A bottom-up model of oil evaporation was constructed using these comprehensive oil composition measurements, avoiding the extensive parameterizations on boiling points and lumping of species typical to oil evaporation models. Accurate prediction of this single weathering process combined with complete composition measurements immediately begins to elucidate all weathering processes that have occurred prior to sampling, providing insights into the probable chemistry and transport of oil occurring after release to the marine environment. Evolution in composition can also be further related to transformation in oil properties that determine the fate of oil (e.g., viscosity). The ability to model the component distribution of fresh and moderately weathered oil presents significant progress in prediction of the fate and environmental impacts following an oil spill.

The rest of this manuscript will begin with a description of explicit calculation of oil evaporation and a brief comparison to existing methods, showing the utility of complete composition measurements. Samples of *MC-252* oil and two surface slicks are then described, as well as the methods used to fully characterize all hydrocarbons in the C_{10}–C_{30} range. Next, experiments on evaporation of simple oil surrogates in a wind tunnel, for the purpose of model validation, are described. Results are then presented demonstrating the accuracy of the evaporation calculations for oil released from the damaged Macondo well and simple mixtures. The application of the model to actual DWH surface slick samples follows, including insight into transport of the spilled oil and potential SOA and ozone formation.

2. Experimental Methods and Materials

2.1. Evaporation Model

The process of evaporation from a pool of liquid is governed by the equation:

$$dM_i/dt = -k_{mass_i}[\mu, MW_i] * \chi_i[t] * \gamma_i * P_{vap}\left[\Delta H_{vap_i}[T]\right] * MW_i * A_{spill}[t] \quad (1)$$

where dM/dt is the mass loss rate, k_{mass} is the mass-transfer coefficient, μ is wind speed (m/s), MW is molecular weight, χ is mole fraction, γ is activity coefficient, P_{vap} is the vapor pressure at 298 K weighted by the

enthalpy of vaporation H_{vap} according to the Clausius-Clapeyron relation, and A_{spill} is the area of the spill surface. Each term in equation (1) with a subscript *i* indicates a quantity specific to species *i*. A long line of research on the evaporation of oil spills from MacKay et al. provided a very thorough and elegant use of dimensionless parameters analogous to a Henry's Law term (H) and evaporative exposure (θ) [*Stiver and Mackay*, 1984; *Mackay and Matsugu*, 1973]:

$$dF_v/dt = k\ a\ P\ v/V_0RT \tag{2}$$

$$dF_v = H\ d\vartheta \tag{3}$$

where dF_v/dt is the volume loss rate of bulk oil, k is the mass-transfer coefficient, a is the spill area, P is the oil vapor pressure, v is oil's molar volume, V_0 is the initial spill volume, R is the ideal gas constant, and T is temperature (K). While this approach immediately gives insight into the physical parameters governing oil evaporation in a straightforward manner, it relies on estimates of properties of the bulk oil. In particular, a reasonable value must be estimated for the molar volume, and the H term is estimated from distillation curves of the bulk oil, both of which can vary significantly with the type of oil and extent of weathering. A recent and updated treatment by Gros et al. parameterizes two-dimensional chromatograms (obtained with flame ionization detection) to predict evaporation, also including slick spreading dynamics [*Gros et al.*, 2014]. Our new analysis technique, GC-VUV-HR-ToFMS, provides a direct measurement of the oil composition in terms of the key parameters governing volatility of hydrocarbons: molecular weight (MW), double bond equivalency (DBE), and branching, and this allows explicit treatment of oil composition using known properties of each species, or from log-linear fits from available data. Because each species is now treated individually, the parameters of H and θ are not needed. For the purpose of applying thermodynamic data, the range of hydrocarbon types were grouped into six categories: linear, branched, mono-cyclic, branched mono-cyclic, poly-cyclic, and aromatic (alkyl benzenes and PAH's). Equation (1) was integrated using basic Euler forward integration, propagating the oil composition by multiplying the derivative as specified in equation (1) by a short time, Δt, to calculate changes in mole fraction, $\Delta\chi_i[t]$, for all oil components: $\chi_i[t+1] = \chi_i[t] + dM/dt[t] * \Delta t$. To accurately capture evaporation for the very volatile components of the oil, Δt was set to between 15 min and 1 h.

Vapor pressure and enthalpy of vaporization data for all available carbon numbers within each class of species was gathered from the NIST web book [*Burgess*, 2015]. Branched compounds for a given carbon number and DBE were assigned, as a class including all isomers, a vapor pressure twice that of the corresponding unbranched compounds; this was estimated from the limited data available for alkane isomer vapor pressures. While branching on the alkyl side-chains of aromatic compounds may affect vapor pressures, their aromatic character more strongly determines the vapor pressure and data were not available for these branched compounds, so no adjustment was made.

Mass-transfer coefficients for all species are determined by relation to that of toluene:

$$k_{mass_i} = k_{mass,Toluene}\sqrt{MW_{Toluene}/MW_i}^{2/3} \tag{4}$$

where the square root of the molecular weights (MWs) accounts for the dependence of diffusivity on molecular weight (MW) and the 2/3 power is a standard dependence of mass-transfer coefficient on diffusivity [*Mackay and Matsugu*, 1973]. The ease of direct toluene measurements enables in situ determination of its gas-phase concentration and thus mass-transfer coefficient, and this can eliminate the need to rely solely on wind speed parameterizations for mass-transfer coefficients, allowing more accurate estimates of evaporation kinetics at spill sites. In wind-tunnel measurements (see below) the mass-transfer coefficient for toluene is measured directly during evaporation experiments using gas-phase measurements, and this toluene-derived mass-transfer coefficient then yields the mass-transfer coefficients for all other species.

2.2. DWH Spilled Oil Samples

Wellhead oil from the DWH is from the Mississippi Canyon reservoir (MC252), and is a sweet light crude, with low sulfur and low viscosity (relatively low resin and asphaltene content) [*Reddy et al.*, 2012]. Samples of surfaced oil from the DWH rig were collected during spill response efforts as described by *Aeppli et al.* [2012]. Sample S2 is a relatively fresh oil collected 36 km due south of the DWH site, and sample S3 is moderately aged oil collected from an oil slick near the coast of Louisiana 130 km northwest of the DWH site. S2

was collected 42 days after the initial blowout; S3, 29 days. These and further details are included in the previous publication by *Aeppli et al*. [2012].

2.3. GC-VUV-HR-ToFMS Analysis of Spilled Oil Samples

The analysis of the oil composition is reported elsewhere; only a brief description of the chromatographic system and quantitation is given here [*Worton et al*., 2015]. DWH oil samples were analyzed using direct injection into a GC system (Agilent) with a high-resolution time-of-flight mass spectrometer (TofWerk). The GC column enabled separation by boiling point (Restek,Rxi 5Sil, 60 m). The HR-ToF was specially modified to pass a vacuum ultraviolet beam (10.5 eV) into the ion-source region, giving soft ionization and low fragmentation of ions. Analysis was carried out at the Chemical Dynamics Beamline (9.0.2) at the Advanced Light Source in Lawrence Berkeley National Lab (Berkeley, CA, USA). Authentic standards were used for calibration for a range of compounds including n-alkanes, branched alkanes, cyclic alkanes, alkyl-benzenes, PAHs, hopanes, and steranes. Calibration methodology was based on the response of the molecular ion as described in previous work [*Worton et al*., 2015; *Isaacman*, 2012; *Chan et al*., 2013]. Deuterated compounds were used as internal standards for response factor determination. All data processing and visualization of GC-VUV-MS data were performed using custom code written in Igor 6.3.6 (Wavemetrics) adapted from high-resolution analysis of high-resolution time-of-flight mass spectrometer data [*DeCarlo et al*., 2006].

2.4. Wind Tunnel

Wind-tunnel experiments were performed to verify that our model accurately reproduces evaporation kinetics for a mixture of hydrocarbons spanning a wide range in volatility. Hydrocarbon mixtures were evaporated in a wind tunnel, shown schematically in Figure 1, with a 12 in. square cross section 10 ft in length, with an attached fan rated up to 400 scfm. Two steel screens (hole diameter 0.25 in., 60% open space) were used to ensure a uniform wind velocity profile, one at the tunnel entrance and one 14 in. downstream. A hot-wire anemometer was used to verify a uniform velocity profile ($<$10% variation through the tunnel cross section) for all operational wind speeds. Hydrocarbon mixtures were added to an aluminum-dish 7 cm in diameter and 28 in. downstream from the tunnel entrance. Five to 12 mL of a liquid-hydrocarbon mixture (below) was used giving a thickness of 1.30–2.60 mm; as will be shown later, measurement-model comparison suggests that mass transfer in the liquid mixture has minor effects even for the most volatile compounds (i.e., toluene). During the course of the experiment, the liquid-hydrocarbon mixture always covered the surface of the dish, maintaining a constant surface-area for evaporation. Temperature was monitored during each evaporation experiment, with variation in room temp generally within several degree Celsius. A thermocouple probe placed underneath the dish verified its temperature was the same as the air temperature. The dish was placed on the bottom of the wind tunnel with an upstream platform, also on the bottom of the tunnel, to create 14 in. of flat surface at the level of the dish, to reduce flow disturbance effects at the leading edge of the dish. HC mixtures were evaporated for periods between 24 and 100 h, to cover the majority of mass evaporation (i.e., allow nearly all the volatile and most intermediate-volatility material to evaporate). Fifty microliter aliquots were periodically removed from the dish for GC analysis. Evaporation experiments were performed using mixtures of five hydrocarbons: toluene (Fisher, HPLC-grade), decane (Sigma-Aldrich, 99%), dodecane (Spectrum, 99%), tetradecane (TCI, 99%), and nonadecane (Spectrum, 99%). The composition of the mixtures (in mass %) was approximately: toluene (3.5%), n-decane (12%), n-dodecane (19%), n-tetradecane (58.5%), and n-nonadecane (7%). This mixture composition spans the range of volatilities necessary for evaporation experiments at 20°C over the course of 150 h, with the extents of evaporation for *n*-alkanes with 10, 12, 14, and 19 carbons ranging from 100%(C_{10}) to less than 5%(C_{19}).

2.5. PTR-MS Analysis

During evaporation experiments the concentration of gas-phase toluene was measured in real-time using a proton transfer reaction mass spectrometer (PTR-MS) with a quadrupole mass analyzer (Ionicon Analytik). Briefly, the PTR-MS creates high levels of H_3O^+ ions by passing water vapor through a hollow cathode ion-source, and the produced H_3O^+ ions transfer protons to (ionize) analytes with proton affinities greater than that of water. Toluene has a proton affinity (187.4 kcal/mol) much higher than that of water (165.2 kcal/mol), making it amenable to PTR-MS detection. A probe for the PTR-MS consisting of 1/4 in. teflon tubing was inserted 32 in. downstream of the oil evaporation dish. The ability to directly measure toluene in the gas phase at high time resolution enables an independent determination of mass-transfer coefficients

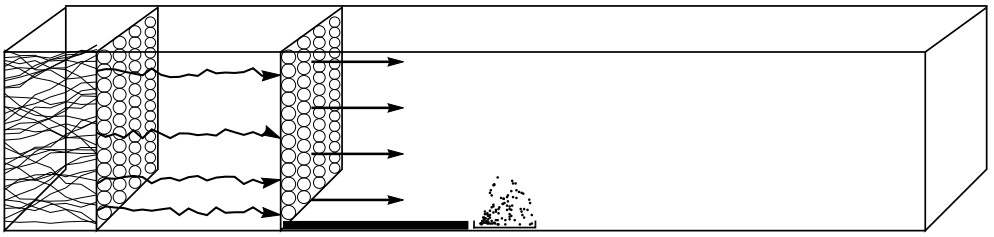

Figure 1. Diagram of wind tunnel used in evaporation experiments.

during evaporation experiments. Thus, there is not a single wind tunnel mass-transfer calibration, but rather each experiment includes a measurement of the toluene mass-transfer coefficient.

2.6. GC-FID Analysis

Samples of initial, final, and during-evaporation aliquots were analyzed via GC-FID. A 5 m column (0.25 mm id, 0.25 m film, Restek, Rxi-5 ms) was used with a temperature program of 40°C with a 5 min hold, followed by a 10°C/min ramp up to 300°C; the carrier gas was H_2 at constant flow of 2 mL/min. The mass ratios of the components of the HC mixture were determined by integration of chromatographic peaks using Chemstation software. Relative sensitivity factors for alkanes were determined using authentic standards (Accustandard C_8–C_{32}).

3. Results and Discussion

3.1. Model Evaluation: Mass Loss of Crude Oil

The performance of the evaporation model can be assessed in terms of two critical aspects of the oil: mass and composition. As discussed above, empirical models can fairly accurately predict mass loss of oil, but they are based on approximations of bulk properties for the comprehensive oil composition (e.g., molar volume). The model presented in this work exploits our detailed oil composition measurements [*Worton et al*., 2015] to predict oil evaporation with minimal or no parameterizations and few assumptions on component volatility.

Evaporation of DWH oil has been previously studied using established measurements of mass loss in a wind tunnel equipped with an analytical balance [*Federal Interagency Solutions Group and Team*, 2013]. These results for total mass loss of DWH crude oil are shown in Figure 2 along with our model predictions, exhibiting excellent agreement between independent measurements and our complete-composition evaporation model. A mass-transfer coefficient of 0.0021 m/s was reported for toluene in the previous measurements, and the current model shows best agreement using $k_{mass} = 0.0025$ m/s for toluene, within uncertainty of the previous measurements. The composition and volatility (aliphatic, aromatic, etc.) of material with fewer than 10 carbons is constrained by measurements from *Reddy et al*. [2012], giving an alkane-dominated composition with an effective average carbon number of 7.7. For evaporation with the specified mass-transfer coefficient, the mass-evaporation kinetics can be considered on two time scales: less than and greater than 30 h. The first ~30 h of evaporation are strongly affected by components with fewer than 13 carbons, though compounds C_{13} and larger have significant emissions as well; further evaporation is dominated by components with greater than 13 carbons. As later discussion will include evaporation at sea, it should be noted that this mass-transfer coefficient is significantly less than 0.01, a value typically used in open-sea modeling for average conditions [*Boehm et al*., 1982; *Stiver et al*., 1988].

3.2. Model Evaluation: Composition Evolution of Representative Mixtures

Wind tunnel experiments were performed to verify model skill with respect to changes in oil composition during evaporation. Figure 3 shows data for an evaporation experiment at 3 m/s wind speed and 21°C using the following hydrocarbons with mass percentages in parentheses: toluene (3.5%), n-decane (12%), n-dodecane (19%), n-tetradecane (58.5%), n-nonadecane (7%). As mentioned above, this composition covers the full volatility range for observing evaporation over a few days. The GC measurements of the composition of the liquid remaining after evaporation are shown as colored points, and the corresponding line of the same color shows the model predictions for the liquid composition. There is excellent agreement between the model predictions and measurements. In addition, the gas-phase PTR-MS signal for toluene,

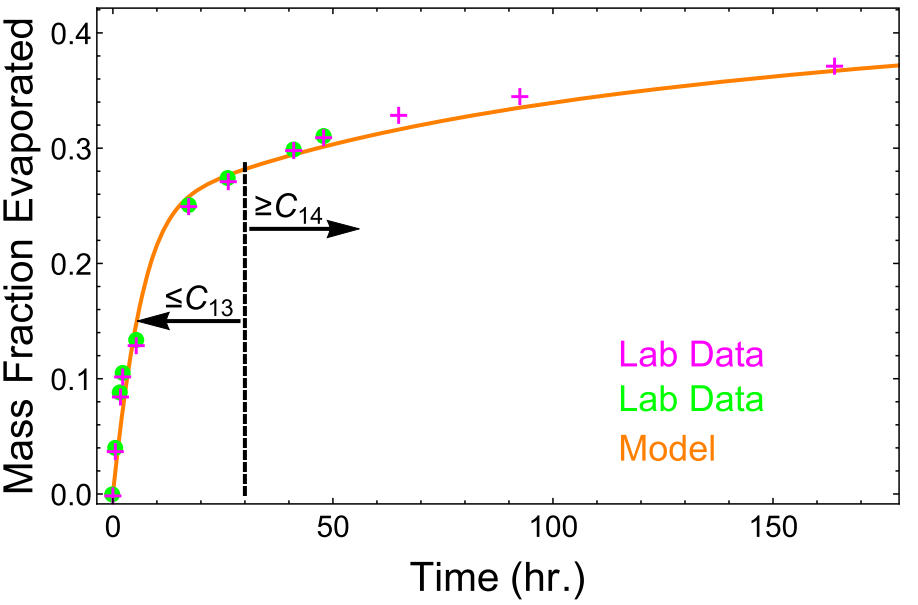

Figure 2. Measurement-model comparison of wellhead oil evaporation. Replicate experimental data in green and pink are from SL-Ross [*The Federal Interagency Solutions Group, Oil Budget Calculator Science and Engineering Team*, 2013]; predictions from bottom-up model are shown in orange.

which is proportional to the mass loss of toluene (the only compound quantified by PTR-MS), and model predictions of toluene loss are shown in the top right of Figure 3. This separate determination of the mass-transfer coefficient further demonstrates the model's ability to accurately predict mass fluxes of evaporating hydrocarbon mixtures.

3.3. Model Applications and Insight to Crude Oil Weathering Processes

3.3.1. Composition Evolution of Crude Oil During DWH Spill

The key advances in this work are: (1) the application of newly possibly comprehensive complete crude oil composition measurements, and (2) prediction of the comprehensive evolution of spilled oil composition as a function of evaporation. Above we demonstrated that total mass loss can be predicted directly by

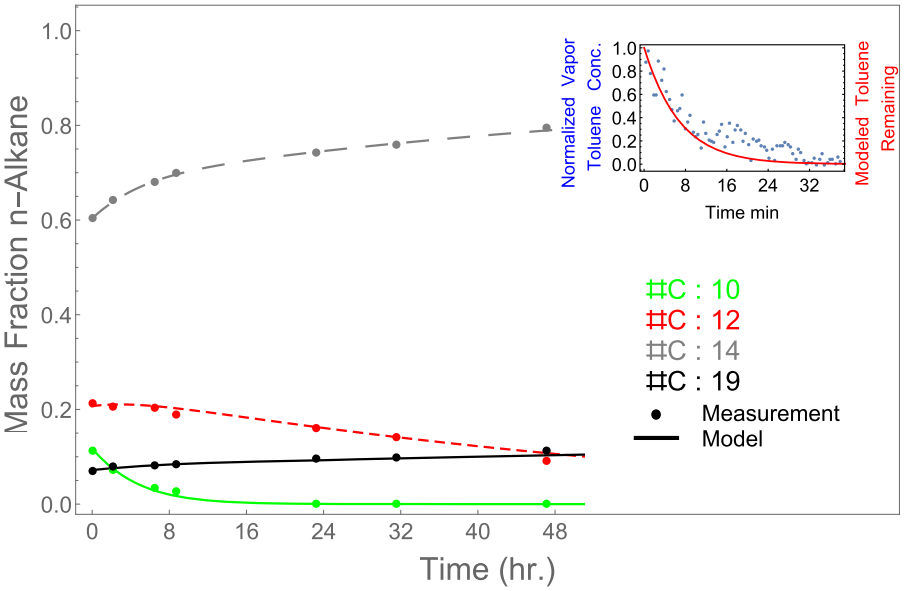

Figure 3. Comparison of time evolution of hydrocarbon mixture of toluene and C_{10}, C_{12}, C_{14}, C_{19} alkanes and the evaporation model. PTR-MS measurements are shown in the top right.

Table 1. List of Model Scenarios and Conditions

Scenario	μ_{eff} (m/s)	Slick Thickness	Age Distribution	Oil Temperature
DWH/S2/29	4.0	Variable	29 h (100%)	35°C
DWH/S2/Dist	4.0	Variable	0.5 h (65)|12–16 h (20)|20 + h (15)	35°C
DWH/S3/Dist	4.0	Variable	0.5–1.5 days (80)|4.8 days + (20)	35°C
Mass Fluxes	4.0	0.5 mm	24 h	25°C
PSOA/Ozone	4.0	0.15 mm	48 h	35°C

modeling evaporation using complete composition measurements, and that simple mixtures covering a wide range of volatilities are also accurately modeled. Now we move to applying the model to environmental samples obtained during the DWH disaster.

First, we compare model results for sample S2, with key model parameters shown in Table 1 as scenario *DWH/S2/29*. Because of the proximity to the DWH wellhead, site S2 should be fairly well constrained in terms of oil transit time to the sampling site via surface currents. Based on available estimates, an average surface drift velocity of 0.35 m/s was assumed, giving an estimated evaporation time scale of 29 h for S2 [*Jolliff et al*., 2014]. The mass-transfer coefficient in this scenario corresponds to 4 m/s average wind speed ($k_{mass} = 0.016$ m/s). Slick thickness is also an important, if uncertain, parameter affecting the evaporation rate, because thinner slicks have a larger surface area per mass of oil. Guided by available estimates [*Leifer et al*., 2012], the slick thickness is set to 500 μm for 0–12 h, 100 μm for 12 to 24h, 10 μm for 24–36 h, and 1 μm for 36+ h. Surface wind speeds in April in the region of the DWH spill are expected to be 2–5 m/s, so this mass-transfer coefficient is comparable to what would be expected [*Daling et al*., 2014]. Model results are shown in Figure 4, comparing the postevaporation composition of the wellhead oil to the surface slick sample S2. In Figure 4, measurements of the source oil (a) and surface sample S2 (b) show that the most volatile components rapidly evaporate, and are thus not present in the surface sample. The peak in the mass distribution moves from $<C_{10}$ to about C_{15} as the oil is weathered. The model results assuming 29 h of evaporation (c) show clear differences from the measured distribution for sample S2. The measurements show persistence of material with 10 carbons at S2, while the model shows that evaporation would completely remove C10 compounds well within 29 h. More specifically the model shows that thermodynamic evaporation will produce the observed mass distribution for material larger than C_{15} only after C_{10} compounds are completely depleted. Notably, the time scales for evaporation from our model are in agreement with measurements of laboratory evaporation of *MC-252* crude oil, showing near complete loss of material $\leq C_{12}$ on similar or even shorter time scales, depending on wind speed conditions [*Daling et al*., 2014]. The source oil distribution will be altered due to dissolution as it rises through the water column prior to evaporation, but in general compounds that dissolve in the water column during the rise to the surface would evaporate on time scales less than the time of sampling (∼10 h), making effects on the final distribution at S2 minor. This comparison of the measured mass distribution and that predicted due to evaporation alone suggests that the material sampled at site S2 has a distribution of lifetimes, with some fraction of the sampled oil reaching the sampling site after minimal evaporation and some reaching S2 after a period of evaporative exposure equal to or longer than the expected transit time from the spill site.

A distribution of evaporative ages can be treated by mixing modeled compositions that result from different durations of evaporation. This is accomplished by fitting the measured mass distributions using a basis set of mass distributions, each of which having a different evaporative age. Basis functions are created by propagating evaporation of our starting DWH composition to span the maximum range of expected surface transport times. Basis set distributions correspond to the composition distribution at regular intervals over the full range of evaporative ages. For example, the basis set for S2 includes oil compositions at 15 min intervals from 0 to 29 h. The modeled final distribution is a linear combination of the individual basis set functions, determined from linear regression with the constraint that all coefficients are greater than or equal to zero. We use the minimal number of basis set functions that achieve a sum of residuals (between the fit and measurements) near the global minimum; this is done by testing the sensitivity of the sum of residuals to the number of basis set functions. All the basis functions are normalized (sum to unity), so the resulting age distribution is determined directly from the fit coefficients for the basis functions.

Measurements of the surface slick composition of samples S2 and S3 are shown in Figures 5 and 6 along with accompanying model results for evaporation of DWH oil. Comparing the relatively fresh (S2) and moderately

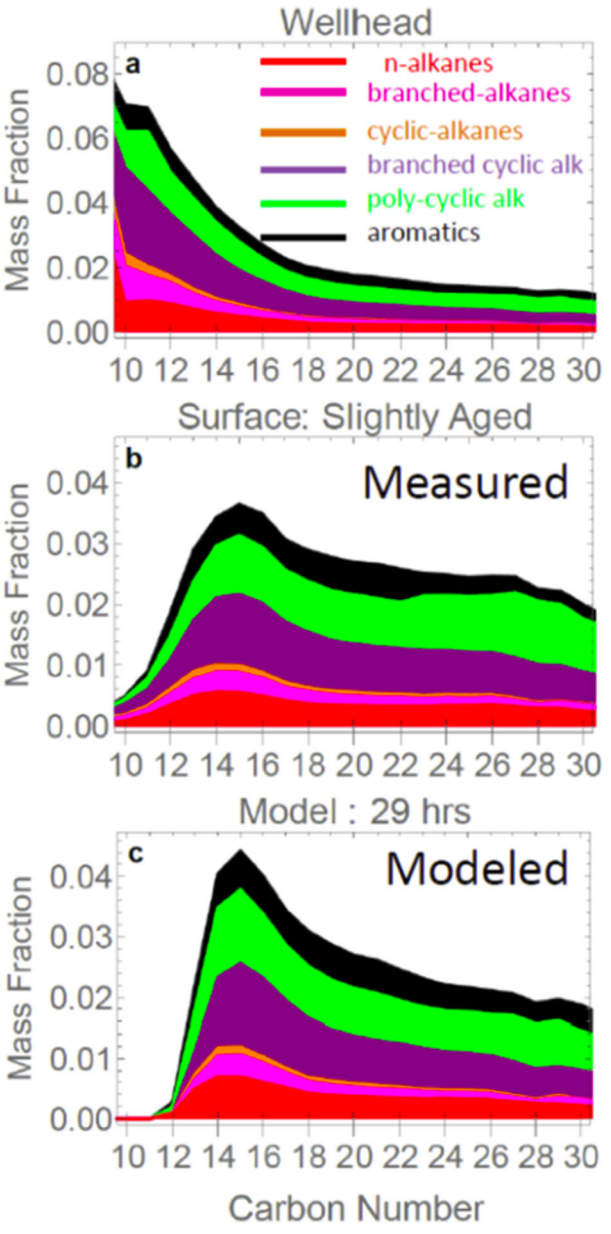

Figure 4. Mass distributions by chemical class for three cases: (a) measured source composition, (b) measured surface composition at S2, (c) modeled composition with 4 m/s wind after 29 h. Colors correspond to hydrocarbon classes: n-alkanes (red), branched linear alkanes (magenta), monocyclic alkanes (orange), branched monocyclic alkanes (purple), bicyclic and tricyclic alkanes (green), polycyclic aromatics and alkyl benzene compounds (black).

aged oil measurements (S3), it is clearly seen that the distributions shift toward less volatile, higher carbon number components. Key model parameters of temperature and wind speed and are shown in Table 1. Slick thickness was time-dependent and treated as described above. An average wind speed of approximately 4 m/s mass was used, which was parameterized by a mass-transfer coefficient of 0.016 m/s. This value is similar to that used by Boehm et al. (0.01 m/s) in modeling the Ixtoc I spill of 1979, also in the Gulf of Mexico [*Boehm et al.*, 1982]. The measured composition at sampling site S2 was best modeled by 65% of the material having an evaporative age of 0–5 h, 20% with an age of 12–16 h, and 15% with an evaporative age of 29+ h. For sampling site S3, we determined 80% of the material has an evaporative age of 0.5–1.5 days and 20% with an evaporative age of 5+ days. Oil composition after 5 days becomes relatively stable to evaporation, so the composition with an evaporative age of 5 days would represent any oil with an age greater than 5 days present at the sampling sites. The fits are not substantially improved by adding basis functions and become substantially worse by further reductions in these ranges, suggesting that the measured distributions are well characterized and require the presence of material with these approximate distributions of evaporative ages. The obtained distributions clearly indicate that fresh oil either recently arrived at the S2 and S3 sites or some fraction of the oil present had experienced strongly hindered evaporation.

Two types of pathways for transport of oil from the wellhead to the sampling site S2 can reasonably explain the estimated distribution of ages: direct transport along the water surface from the immediate vicinity of the DWH wellhead and subsurface transport from the wellhead to very near S2. *Aeppli et al.* also noted that the presence of $<C_{10}$ material at site S2, suggesting the sampled oil had recently surfaced [*Aeppli et al.*, 2012]. Any process hindering evaporation (e.g., emulsion formation) could enhance the fraction of fresh (short evaporative age) oil at S2, but the clear presence of material C_{10} and smaller requires that some fraction of the oil has an evaporative age of less than 2 or 3 h, which can only be reasonably explained by subsurface transport. A shorter transit time would be correlated with faster winds and enhanced evaporation

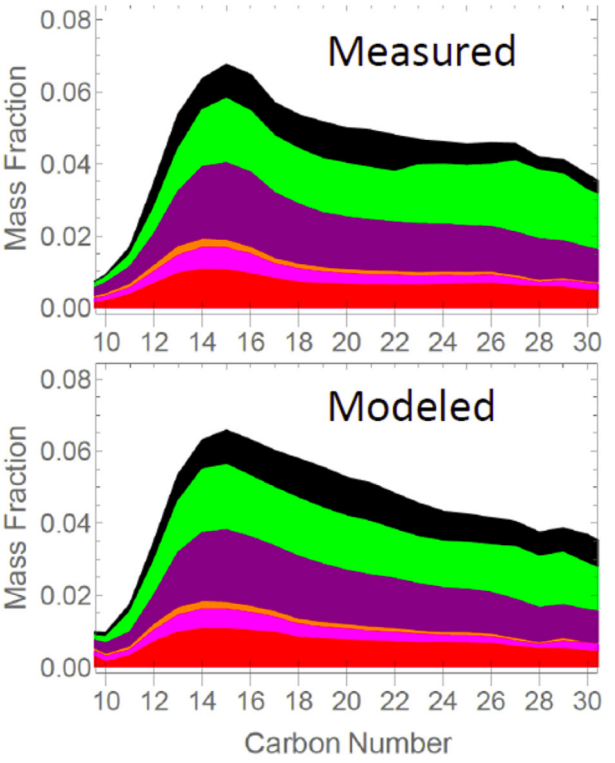

Figure 5. (top) Mass distributions by chemical class for surface composition (S2) measured by GCVUV-HTOFMS, and (bottom) modeled with 4 m/s wind with an evaporative age distribution (<5 h 60%, 12–16 h 25%, 29+ h 15%). Colors correspond to same classes as in Figure 4.

and can thus be ruled out. Plume dynamics for deep-sea blowouts have shown that probable droplet size distributions can result in intrusion layers and lateral subsurface transport, even without application of dispersants [*Socolofsky et al.*, 2011]. Surfacing distances can be up to a hundred kilometers or more for smaller (sub-mm) droplets leading to a wide range of surfacing distances up to hundreds of kilometers [*North et al.*, 2015]. *Ryerson et al.* [2012] determined via aircraft measurements that almost all oil surfaced within 2 km of the DWH site, differences in the results presented here may be due to the fact that the aircraft measurements were made a week or later after the "top hat" cap was applied to the leaking wellhead, which may change plume dynamics. Linking sampled oil composition to its weathering history is significant because it presents an independent constraint for models that incorporate plume dynamics and ocean currents.

Several sources other than subsurface transport may also contribute to differences between the model and measurements. The oil continuously spilled and surfaced, so transit times/paths to the sampling site will vary with wind speed and direction. The formation of a "skin" of heavier, possibly more polar, components at the oil-air interface has been proposed to hinder evaporation of lighter oil components [*Fingas*, 2011]. Dissolution, formation of emulsions, bubble bursting, and particularly photochemical oxidation are other processes that occur at sea with complex effects on transformation of the oil's mass distribution. Recent data from *Bacosa et al.* [2015] show the lifetime of aromatic/PAH compounds above C_{10} is, on average, about 5 days. This is in reasonable agreement with our measurements, which show roughly 50% loss for low volatility aromatics after 5 days. Our model shows losses for aromatics above C15 to be much lower, 0–25%. Guided by the current experimental results, the difference between our measured and modeled aromatic fractions can be attributed to photodegradation. The persistence of the more volatile material in samples S2 and S3 is clearly indicative of a combination of varying transit times and the listed nonevaporative processes. Furthermore, the slick thicknesses used are likely upper estimates; if the slick was in fact thinner, this would further support the conclusion of subsurface transport.

3.3.2. Mass Fluxes

Petroleum hydrocarbon emission rates, including speciation, are a key factor that determines the atmospheric concentrations, rate of formation of secondary atmospheric pollutants, and hence exposure levels. Emission rates are strongly coupled to environmental conditions such as temperature and wind speed and also vary greatly with oil composition. Furthermore, the oxidation processes that follow hydrocarbon emissions and lead to SOA are coupled to conditions such as solar flux (zenith angle and cloud cover). Because all aspects of pollutant formation will depend on environmental conditions that may change on short time scales, accurate prediction of pollutant formation requires good estimate of temporal changes in mass fluxes. Speciation of emissions is important because the formation of SOA and ozone due to atmospheric processing of hydrocarbons varies strongly with structure. The key factors are: carbon number, branching, cyclization, and aromatic content [*Hallquist et al.*, 2009; *Odum et al.*, 1996; *Tkacik et al.*, 2012; *Ng et al.*, 2007; *Gentner et al.*, 2012; *Jordan et al.*, 2008; *Cappa et al.*, 2013; *Jimenez et al.*, 2009].

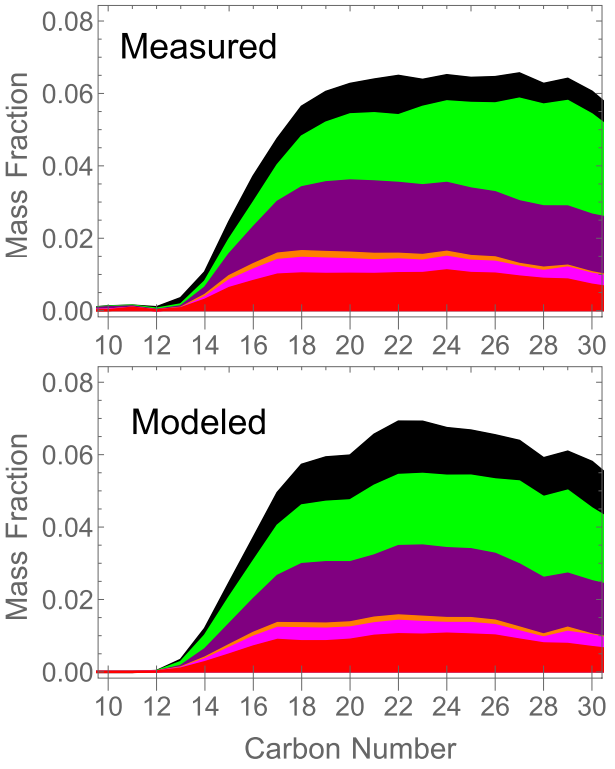

Figure 6. Mass distributions by chemical class for (top) composition of surface sample from S3 measured by GC-VUV-HR-ToFMS, and (bottom) modeled distribution with 4 m/s wind with an evaporative age distribution of 0.4–1.4 days (80%) and 4.8+ days 20%. Colors correspond to same classes as in Figure 4.

Most oil spill models predict mass loss without significant speciation (e.g., GNOME, ADIOS, OilTrans), and models with greater speciation rely on reasonable surrogate classes with representative properties (i.e., groups of compounds are assigned a single vapor pressure). The information from our GC-VUV-HR-ToFMS analysis allows explicit inclusion of species according to carbon number, structure (double bond equivalency), and branching. This higher level of speciation is the hallmark of the model presented here, in particular because this level of speciation can be directly related to yields of key atmospheric pollutants (ozone, organic aerosol) and key oil properties (viscosity, density, etc.)

The calculated mass fluxes for a spill of DWH oil at the sea surface are shown in Figure 7, including n-alkanes, branched alkanes, and aromatic species with carbon numbers 10, 11, 12, and 14. Fluxes for C_{14} have been multiplied by a factor of 10 for clarity. Details of the environmental parameters used are shown in Table 1 as scenario *Mass Fluxes*. The fluxes are shown normalized to the maximum flux for the corresponding C_{10} compound of the same hydrocarbon class, the magnitude of which is indicated in the top left corner of each plot. Peak magnitudes of the mass fluxes are quite large on a per-area basis, with several g/h/m^2 emissions of C_{10}–C_{12} compounds occurring over several hours for light crudes such as *MC-252*. Larger compounds show smaller but sustained emissions over much longer periods. More specifically, C_{10} species dominate emissions for the first 1.5 h; C_{11}, 3.5 h; C_{12+} >3.5 h. The modeled fluxes directly indicate the evaporation lifetimes, which are in agreement the results of with *Delvigne*, who observed a half-life of <3 h for C_{10} compounds and <4 h for C_{12} compounds in field experiments with comparable wind speed and oil composition [*Delvigne*, 1985]. A recent field and modeling study involving release of Grane heavy crude oil in the North Sea as a thin oil sheen with thickness <10 μm showed >50% loss of C_{16} within 1 h and C_{17} within 25 h [*Gros et al*., 2014]. For comparison, the current model was run for a slightly modified DWH oil, enhancing >C_{34} compounds to 40% of total oil mass. We predict comparable lifetimes for 50% loss (C_{16}: 5h, C_{17}:24 h) to those of Gros et al. This is good agreement given that the low carbon number mass distribution data for Grane crude oil were not available.

To show the effects of changing oil composition on mass fluxes, our model was applied to a hypothetical oil, which has the composition of DWH oil excluding material below C_{10}. These results are shown in Figure 8 and environmental conditions are given in the *Mass Fluxes* scenario in Table 1. Comparing the DWH oil with this truncated, hypothetical distribution, it is clear that temporal trends remain largely the same, but the peak fluxes increases by ∼35% in all cases. The peak in the surface-spill scenario does not occur at $t = 0$, because the presence of the <C_{10} material initially reduces the effective vapor pressure of the heavier components. This shows that Raoult's law effects (proportionality of vapor pressure to mole fraction composition) can enhance the rate of evaporation of C_{10}–C_{13} compounds significantly, and deep-sea spills will have enhanced rates of evaporation for these compounds if significant amounts of small, soluble components dissolve prior to oil surfacing.

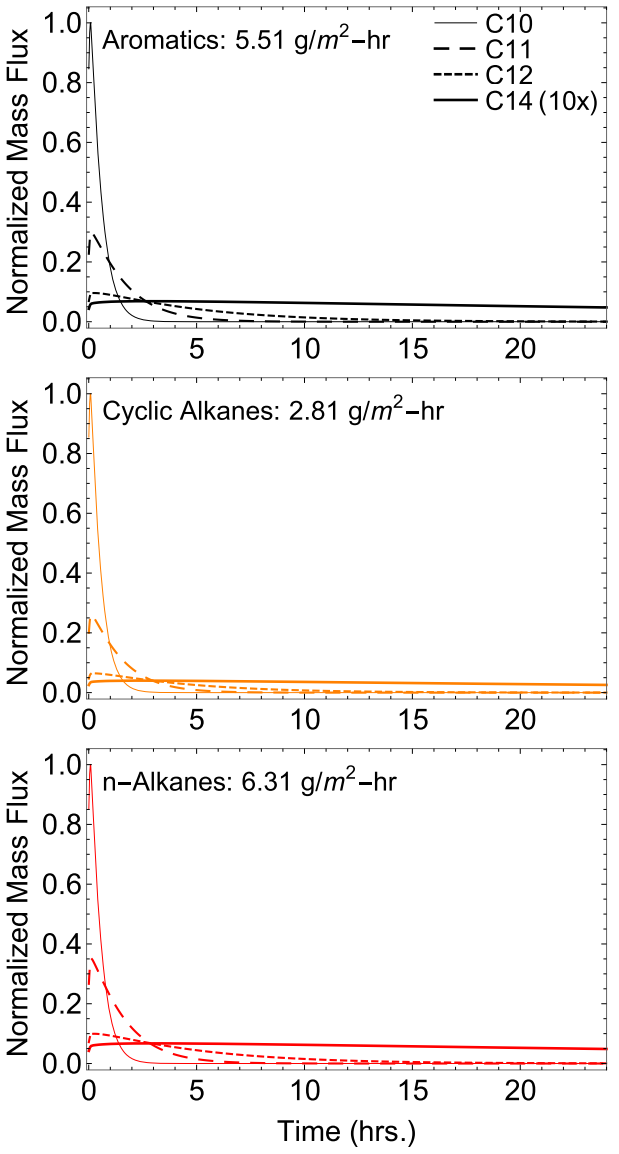

Figure 7. Mass fluxes from three classes of hydrocarbons following a surface release of MC 252 crude: (a) aromatics, (b) cyclic alkanes, and (c) n-alkanes. Slick is 500 μm thick, and wind speed is 4 m/s. All data for a given class are normalized to the maximum flux of the C_{10} compound.

3.3.3. Potential SOA Formation

After release to the atmosphere material is converted to secondary organic aerosol (SOA) by atmospheric oxidation, which lowers its vapor pressure and causes partitioning into existing aerosol, as was indeed observed in the region of the DWH site [*de Gouw et al*., 2011; *Middlebrook et al*., 2011]. Although SOA formation is a dynamic process that is dependent on evolving gas, oxidant, and aerosol concentrations, here we simply estimate the final yield of SOA by applying end point yields to the mass of hydrocarbons emitted, or potential secondary organic aerosol (PSOA) yields. Speciated yields for PSOA as a function of carbon number and DBE, adapted from *Gentner et al*. [2012], were applied to the modeled emissions from *MC-252* oil under conditions similar to those experienced in Gulf of Mexico. Initial estimates were published by *Gentner et al*. [2012] for high-NOx conditions and adapted from Jordan et al. but updated measurements show alkane yields are likely much higher than these original estimates, for both high-NOx and low-NOx conditions [*Tkacik et al*., 2012; *Jordan et al*., 2008; *Cappa et al*., 2013; *Presto et al*., 2010]. To make the PSOA yield parameterizations more representative of current laboratory experiments, linear alkane yields were multiplied by about a factor of six, branched alkanes by about a factor of 7, and cyclic alkanes by about a factor of 10. Aromatic yields were not adjusted. Upper limits for nonaromatics were 1.1. While branched alkane yields decrease with branching at high-NOx, their low-NOx yields have been shown to be slightly greater than for linear alkanes. The yield parameterizations used are given in supporting information Table S1. Below is a discussion of the application of these PSOA yields, prediction of PSOA during different spill scenarios, and a comparison to actual SOA observations and yield estimates for the DWH spill.

Predictions for the total SOA yield from the initial mass of spilled oil are shown in Figure 9 for the conditions specified in Table 1; the color scheme is consistent with the previous mass distributions of the oil. The left and right plots of Figure 9 show PSOA yields for at-depth release (~1500 m), and a surface spill, respectively. The surface spill uses the full composition of the neat *MC-252* oil, while the at-depth release has 50% of the $<C_{10}$ aromatics removed, commensurate with the estimate of *Ryerson et al*. [2011]. First, we examine the at-depth release. The branched cyclic compounds are present at high fractions in the evaporating liquid and also have high yields, making them the dominant class of aliphatic PSOA. The dominance of aromatics at short time scales and aliphatics at longer time scales is also shown in supporting information Figure S1,

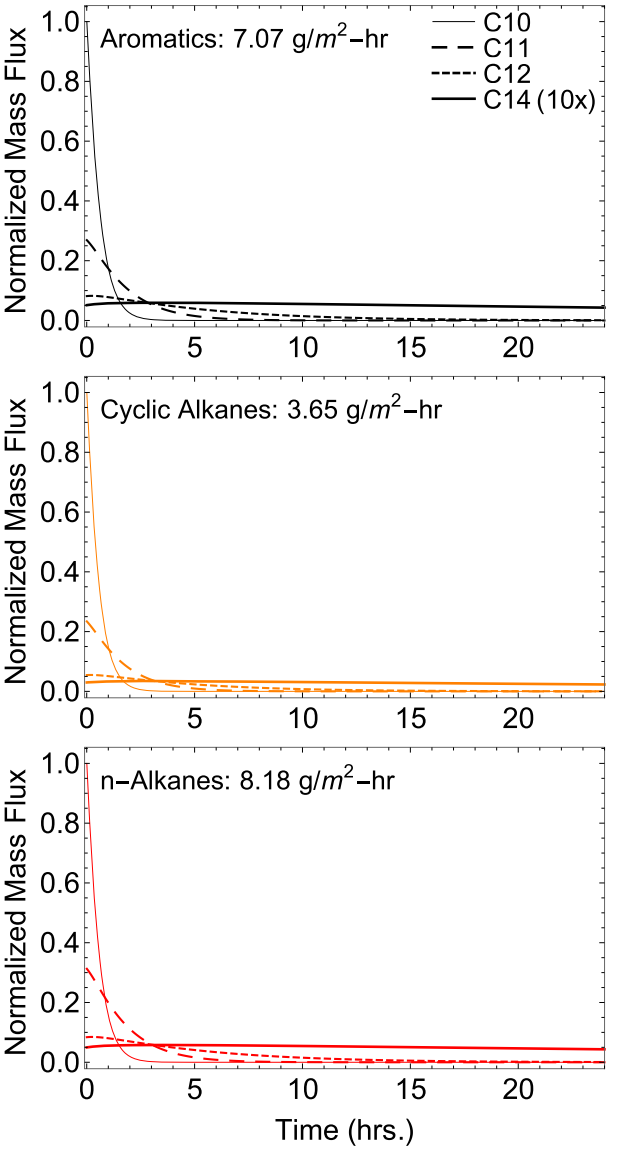

Figure 8. Mass fluxes from three classes of hydrocarbons following a deep-sea release of a hypothetical oil that is MC 252 crude excluding compounds below C10. (a) aromatics, (b) cyclic alkanes, and (c) n-alkanes. Slick is 500 μm thick, and wind speed is 4 m/s. All data for a given class are normalized to the maximum flux of the C_{10} compound.

which shows noncumulative yields. An at-depth release for a light crude oil similar to *MC-252*, with the conditions specified in Table 1 shows a PSOA yield of 6%, in g-PSOA/g-Oil, after 48 h of uninhibited evaporation. The surface-spill shows the same trend, with a slightly higher yield of 6.5% over the same time period, due to the increase in faster evaporating, high-PSOA yield aromatic material. Other variations in oil composition may also lead to rapid PSOA formation, as is indicated above in by the enhanced mass fluxes in Figure 8. Enhanced mass fluxes due to Raoult's law considerations could also lead to significant increases in initial PSOA formation following a spill. It should be emphasized that yields can vary by 50% due to variation in spill conditions, particularly slick thickness, and corresponding changes in evaporative lifetimes. The conditions used here are reasonable given the assumed proximity to the spill site and give SOA yields that are generally consistent with observations.

Detailed modeling of SOA formation is critical in assessing environmental impacts of oil spills on human health. Several additional factors may be important for releases of oil from different sources and in different locations. Evaporation of material that is not GC-amenable (i.e., fairly oxidized material) is not included in this analysis, but these compounds are likely to have very low vapor pressures, as compared to hydrocarbons. Including this material is likely to slightly increase yields, as the potentially higher PSOA yields are balanced by low mass fraction in the weathered oil. Also, evaporation kinetics of the oil, mainly affected by slick thickness and wind speed, will play a large role in the actual concentrations of SOA formed. This requires modeling of the evaporation process before applying the parameterized, compound-specific PSOA yields to the vapors released over a spill. With the massive amounts of oil that may be released from rigs such as the DWH, there is a strong potential for very high levels of SOA to result from the evaporation of crude oil.

The bottom-up estimates of PSOA presented here can be compared with the observations during the spill to better understand the emissions leading to SOA formation. Estimates for SOA formation during the DWH spill made by *Middlebrook et al.* [2011] are somewhat higher and different in terms of composition. *Middlebrook et al.* [2011] estimate 8 ± 4% gSOA/gOil is formed mainly by aliphatic compounds 3 h downwind, and the model results presented here suggest that the aliphatic vapors emitted over the course of three hours will have a PSOA yield of ~3%. The model-based estimate should be an upper limit to the PSOA yield per mass of oil, because it assumes that end point SOA yields are reached instantaneously, whereas the time scale for SOA formation (related to the lifetime for OH oxidation) is on the order of several hours. This

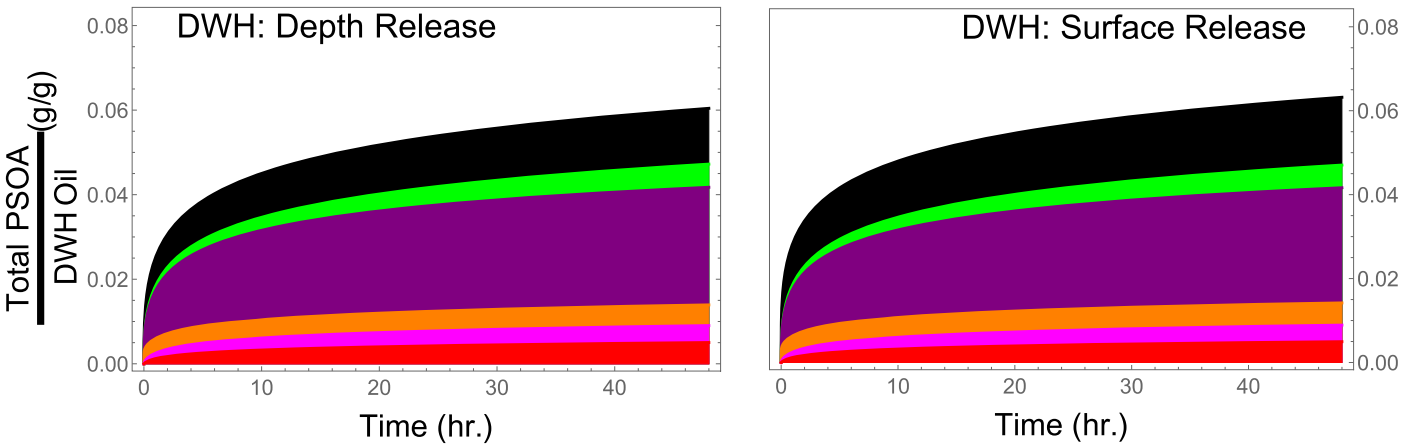

Figure 9. Modeled cumulative yields of potential secondary organic aerosol (PSOA) formation from DHW oil evaporation for two scenarios: (left) release at 1500 m depth, (right) surface spill. Yields are expressed as cumulative mass of PSOA per the initial mass of oil released. The at-depth release is treated by removal of 50% of $>C_{10}$ aromatics from the initial composition. Colors correspond to PSOA derived from the same classes of compounds as in Figure 4.

comparison suggests that a significant fraction of the emissions leading to SOA formation are from oil that previously surfaced. This conclusion is supported by the fact that the model results suggest that freshly released oil will have a significant fraction of aromatic SOA, whereas observations suggest that aromatics did not play a major role in SOA formation [*Middlebrook et al.*, 2011; *de Gouw et al.*, 2011]. The modeled results are also supported by laboratory measurements and detailed composition of the aerosol formed during the DWH disaster that suggest the importance of emissions of IVOC compounds larger than C_{10} [*Bahreini et al.*, 2012; *Li et al.*, 2013]. Previously surfaced oil will have lost nearly all the volatile aromatics predicted to lead to rapid SOA formation. The bottom-up modeling estimates of PSOA yields thus suggest observation based yields per mass of oil released are slightly overestimated and that the observed SOA was formed in part by IVOCs emitted from oil released over more than 1 day.

3.3.4. Ozone Formation

Potential ozone yields were calculated using a method analogous to that of the PSOA; maximum incremental reactivity (MIR) ozone yields were applied to the modeled flux of oil vapors. The MIR scale is used to assess the effect of increasing the gas-phase concentration of an organic vapor on ozone concentrations, expressed as a yield (g-ozone/g-VOC). The MIR scale predicts changes in ozone when conditions are most

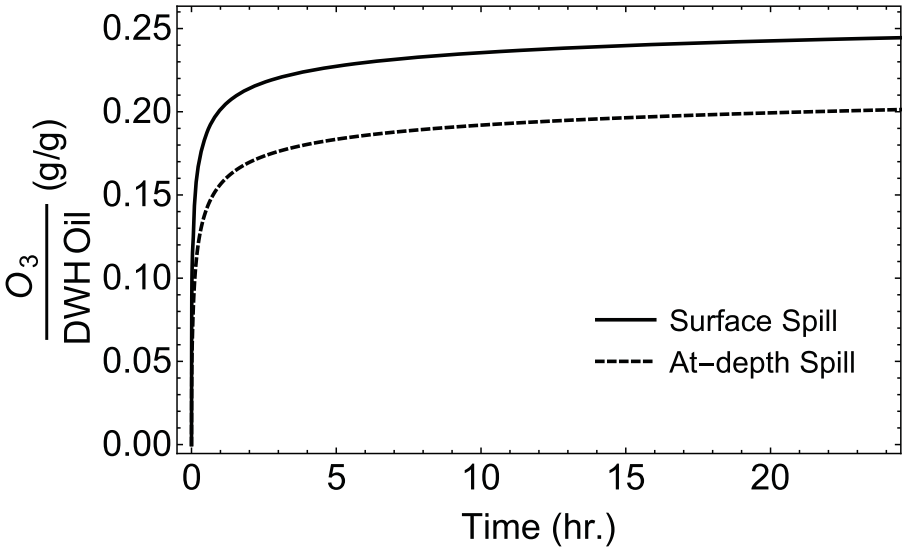

Figure 10. Modeled maximum incremental reactivity(MIR) ozone yields from the DHW oil evaporation for two scenarios: release at 1500 m depth (dashed line) and surface spill (solid line). Yields are expressed as cumulative ozone formation per mass of initial oil released.

sensitive to addition of organics (e.g., VOC:NO_x ratio). Modeling results are shown in Figure 10 for two cases: a deep-release (dashed line) and a surface spill (solid line). The deep-release case, as with PSOA predictions, is treated by removing 50% of the aromatics smaller than C_{10} from the DWH oil composition. In both cases the temporal trend is similar, a sharp burst of ozone initially followed a very slow increase as less volatile material evaporates. There is a clear difference in the amount of ozone formed in the two cases; the surface-spill results in about 20% higher increases in ozone than the deep-release case. This difference is much more pronounced than with PSOA, which showed only about 5% increase for the surface-spill case. These differences in pollutant yields are explained by the trends on carbon nuber and compounds class for MIR and PSOA yields. Aromatics have high MIR ozone yields, between 2 and 8, with the maximum for C_9 compounds, whereas aliphatics have much lower yields (maximum of about 1.5). The MIR ozone yields for aliphatics decrease with increasing carbon number, while aliphatic PSOA yields increase with carbon number. The modeled changes in ozone yields show that oil spills areas with any appreciable level of NO_x will form large amounts of ozone. During a spill, a constant flux of volatile material will be present and lead to sustained, high levels of ozone, while areas with weathered oil will have smaller but sustained yields of ozone.

4. Conclusions

A model for oil evaporation based on comprehensive composition measurements using GC-VUV-HR-ToFMS analysis of crude oil was developed, tested, and applied to fresh DWH crude oil and weathered surface-slick samples from the DWH spill of 2010. Mass loss due to evaporation and the composition of the emitted hydrocarbon vapors are in agreement with previous wind tunnel measurements and new measurements presented in this manuscript. Analysis of two surface samples of spilled oil suggests that multiple transport pathways, likely subsurface and surface, create surface slicks composed of oil with a range of evaporative ages. Using the current model to predict oil composition for various evaporative ages, the distribution of ages present in spilled oil samples in the vicinity (30 km) and farther (130 km) from the DWH rig were calculated. Oil that was very fresh compared to expected transit times was present for both surface-slick sampling sites. S2 (30 km from DWH rig) included oil with an evaporative age of just several hours compared to the expected transit time of 29 h, and S3 (130 km) included oil with an evaporative age of less than 1.5 days compared to an approximate surface transit time of nearly 5 days. Mass fluxes due to evaporation of DWH oil are very large within the first day of evaporation, with peak fluxes for most compounds in the 2–7 $g/m^2/h$ range. For deep-sea blowouts, dissolution of a significant fraction of lighter aromatic compounds during the rise to the surface can have observable effects on peak fluxes for larger (e.g., C_{10}) aliphatics. Potential secondary organic aerosol formation from oxidation of emitted hydrocarbon vapors and subsequent condensation to existing atmospheric particles is significant for DWH oil. Yields of up to 6.5% gSOA/gOil can be attained after 2 days of evaporation (surface spill). Ozone yields for evaporative emissions are 20–25% gOzone/gOil after 24 h. These total SOA yields for bulk oil are strongly related to the oil composition, because the yields for individual oil components can vary by an order of magnitude, particularly for the faster-evaporating compounds ($<C_{14}$). Observations of SOA during the DWH spill show prompt formation of SOA due mainly to aliphatics with a high yield (8%) [*Middlebrook et al*., 2011]. The model presented here indicates that evaporation of aliphatic compounds from an oil slick may reach slightly lower yields.

This work makes clear the importance and utility of comprehensive composition measurements of both fresh oil spill before a spill and weathered oil during an oil spill. Comprehensive composition measurements can effectively constrain transport mechanisms for weathered samples, informing ocean-current models. Utilizing initial comprehensive composition allows prediction of potential pollutant formation and the sensitivity of atmospheric emissions to the type of release (deep sea versus surface spill).

Acknowledgments
This work was supported by the Gulf of Mexico Research Initiative as part of the Gulf Integrated Spill Research Consortium (GISR). Sample analysis by GC-VUV-HR-ToFMS was done at Lawrence Berkeley National Laboratory at the Chemical Dynamics Beamline 9.0.2 at the Advanced Light Source. C. Reddy and C. Aeppli were funded by NSF (OCE-1333148). Composition and sample information has been archived on the Gulf of Mexico Research Initiative Information and Data Cooperative (GRIIDC, data.gulfresearchinitiative.org/).

References

Aeppli, C., C. A. Carmichael, R. K. Nelson, K. L. Lemkau, W. M. Graham, M. C. Redmond, D. L. Valentine, and C. M. Reddy (2012), Oil weathering after the Deepwater Horizon disaster led to the formation of oxygenated residues, *Environ. Sci. Technol.*, *46*, 8799–8807, doi: 10.1021/es3015138.

Bacosa, H. P., D. L. Erdner, and Z. Liu (2015), Differentiating the roles of photooxidation and biodegradation in the weathering of Light Louisiana Sweet crude oil in surface water from the Deepwater Horizon site, *Mar. Pollut. Bull.*, *95*, 265–272.

Bahreini, R., et al. (2012), Mass spectral analysis of organic aerosol formed downwind of the Deepwater Horizon oil spill, *Environ. Sci. Technol.*, *46*, 8025–8034.

Boehm, P. D., D. L. Fiest, D. Mackay, and S. Paterson (1982), Physical-chemical weathering of petroleum hydrocarbons from the IXTOC I blowout: Chemical measurements and a weathering model, *Environ. Sci. Technol.*, *16*, 498–505, doi:10.1021/es00102a014.

Burgess, D. R. (2015), Thermochemical data in NIST Chemistry WebBook, in *NIST Standard Reference Database*, vol. 69, edited by P. J. Linstrom and W. G. Mallard, Natl. Inst. of Stand. and Technol., Gaithersburg, Md. [Available at http://webbook.nist.gov, last accessed 20 Feb. 2015.]

Cappa, C. D., X. Zhang, C. L. Loza, J. S. Craven, L. D. Yee, and J. H. Seinfeld (2013), Application of the statistical oxidation model (SOM) to secondary organic aerosol formation from photooxidation of C12 alkanes, *Atmos. Chem. Phys.*, *13*, 1591–1606, doi:10.5194/acp-13-1591-2013.

Chan, A., et al. (2013), Detailed chemical characterization of unresolved complex mixtures in atmospheric organics: Insights into emission sources, atmospheric processing, and secondary organic aerosol formation, *J. Geophys. Res. Atmos.*, *118*, 6783–6796, doi:10.1002/jgrd.50533.

Chanton, J., T. Zhao, B. E. Rosenheim, S. Joye, S. Bosman, C. Brunner, K. M. Yeager, A. R. Diercks, and D. Hollander (2015), Using natural abundance radiocarbon to trace the flux of petrocarbon to the seafloor following the deepwater horizon oil spill, *Environ. Sci. Technol.*, *49*, 847–854, doi:10.1021/es5046524.

Daling, P. S., F. Leirvik, I. K. Almås, P. J. Brandvik, B. H. Hansen, A. Lewis, and M. Reed (2014), Surface weathering and dispersibility of MC-252 crude oil, *Mar. Pollut. Bull.*, *87*, 300–310, doi:10.1016/j.marpolbul.2014.07.005.

DeCarlo, P. F., et al. (2006), Field-deployable, high-resolution, time-of-flight aerosol mass spectrometer, *Anal. Chem.*, *78*, 8281–8289, doi:10.1021/ac061249n.

de Gouw, J. A., et al. (2011), Organic aerosol formation downwind from the deepwater horizon oil spill, *Science*, *331*, 1295–1299, doi:10.1126/science.1200320.

Delvigne, G. (1985), Experiments on natural and chemical dispersion of oil in laboratory and field circumstances, in *International Oil Spill Conference Proceedings*, pp. 507–514, edited by J. O. Ludwigson, Amer. Petrol. Inst., Washington, D. C.

Fingas, M. (2011), *Oil Spill Science and Technology: Prevention, Response, and Cleanup*, Elsevier, N. Y.

Gentner, D. R., et al. (2012), Elucidating secondary organic aerosol from diesel and gasoline vehicles through detailed characterization of organic carbon emissions, *Proc. Natl. Acad. Sci. U. S. A.*, *109*, 18,318–18,323, doi:10.1073/pnas.1212272109.

Gros, J., D. Nabi, B. Würz, L. Y. Wick, C. P. D. Brussaard, J. Huisman, J. R. van der Meer, C. M. Reddy, and J. S. Arey (2014), First day of an oil spill on the open sea: Early mass transfers of hydrocarbons to air and water, *Environ. Sci. Technol.*, *48*, 9400–9411, doi:10.1021/es4042836.

Hallquist, M., et al. (2009), The formation, properties and impact of secondary organic aerosol: Current and emerging issues, *Atmos. Chem. Phys.*, *9*, 5155–5236, doi:10.5194/acp-9-5155-2009.

Isaacman, G. (2012), Improved resolution of hydrocarbon structures and constitutional isomers in complex mixtures using gas chromatography-vacuum ultraviolet-mass spectrometry, *Anal. Chem.*, *84*, 2335–2342, doi:10.1021/ac2030464.

Jimenez, J. L., et al. (2009), Evolution of organic aerosols in the atmosphere, *Science*, *326*, 1525–1529, doi:10.1126/science.1180353.

Jolliff, J. K., T. A. Smith, S. Ladner, and R. A. Arnone (2014), Simulating surface oil transport during the Deepwater Horizon oil spill: Experiments with the BioCast system, *Ocean Modell.*, *75*, 84–99, doi:10.1016/j.ocemod.2014.01.004.

Jordan, C., P. Ziemann, R. Griffin, Y. Lim, R. Atkinson, and J. Arey (2008), Modeling SOA formation from OH reactions with C8–C17 n-alkanes, *Atmos. Environ.*, *42*, 8015–8026, doi:10.1016/j.atmosenv.2008.06.017.

Leifer, I., et al. (2012), State of the art satellite and airborne marine oil spill remote sensing: Application to the BP Deepwater Horizon oil spill, *Remote Sens. Environ.*, *124*, 185–209, doi:10.1016/j.rse.2012.03.024.

Li, R., B. Palm, A. Borbon, M. Graus, C. Warneke, A. M. Ortega, D. A. Day, W. H. Brune, J. L. Jimenez, and J. A. de Gouw (2013), Laboratory studies on secondary organic aerosol formation from crude oil vapors, *Environ. Sci. Technol.*, *47*(21), 12,566–12,574, doi:10.1021/es402265y.

Mackay, D., and R. S. Matsugu (1973), Evaporation rates of liquid hydrocarbon spills on land and water, *Can. J. Chem. Eng.*, *51*, 434–439, doi:10.1002/cjce.5450510407.

McNutt, M. K., R. Camilli, T. J. Crone, G. D. Guthrie, P. A. Hsieh, T. B. Ryerson, O. Savas, and F. Shaffer (2011), Review of flow rate estimates of the Deepwater Horizon oil spill, *Proc. Natl. Acad. Sci. U. S. A.*, *109*, 20,260–20,267, doi:10.1073/pnas.1112139108.

Middlebrook, A. M., et al. (2011), Air quality implications of the Deepwater Horizon oil spill, *Proc. Natl. Acad. Sci. U. S. A.*, *109*, 20,280–20,285, doi:10.1073/pnas.1110052108.

Ng, N. L., J. H. Kroll, A. W. H. Chan, P. S. Chhabra, R. C. Flagan, and J. H. Seinfeld (2007), Secondary organic aerosol formation from m-xylene, toluene, and benzene, *Atmos. Chem. Phys.*, *7*, 3909–3922, doi:10.5194/acp-7-3909-2007.

North, E. W., E. E. Adams, A. E. Thessen, Z. Schlag, R. He, S. A. Socolofsky, S. M. Masutani, and S. D. Peckham (2015), The influence of droplet size and biodegradation on the transport of subsurface oil droplets during the Deepwater Horizon spill: A model sensitivity study, *Environ. Res. Lett.*, *10*, 024016, doi:10.1088/1748-9326/10/2/024016.

Odum, J. R., T. Hoffmann, F. Bowman, D. Collins, R. C. Flagan, and J. H. Seinfeld (1996), Gas-particle partitioning and secondary organic aerosol yields, *Environ. Sci. Technol.*, *30*, 2580–2585, doi:10.1021/es950943.

Passow, U. (2014), Formation of rapidly-sinking, oil-associated marine snow, *Deep Sea Res., Part II*, doi:10.1016/j.dsr2.2014.10.001.

Presto, A. A., M. A. Miracolo, N. M. Donahue, and A. L. Robinson (2010), Secondary organic aerosol formation from high-NOx photo-oxidation of low volatility precursors: n-alkanes, *Environ. Sci. Technol.*, *44*, 2029–2034, doi:10.1021/es903712r.

Reddy, C. M., et al. (2012), Composition and fate of gas and oil released to the water column during the Deepwater Horizon oil spill. *Proc. Natl. Acad. Sci. U. S. A.*, *109*, 20,229–20,234, doi:10.1073/pnas.1101242108.

Ryerson, T. B., et al. (2011), Atmospheric emissions from the Deepwater Horizon spill constrain air-water partitioning, hydrocarbon fate, and leak rate, *Geophys. Res. Lett.*, *38*, L07803, doi:10.1029/2011GL046726.

Ryerson, T. B., et al. (2012), Chemical data quantify Deepwater Horizon hydrocarbon flow rate and environmental distribution, *Proc. Natl. Acad. Sci. U. S. A.*, *109*, 20,246–20,253, doi:10.1073/pnas.1110564109.

Socolofsky, S. A., E. E. Adams, and C. R. Sherwood (2011), Formation dynamics of subsurface hydrocarbon intrusions following the Deepwater Horizon blowout, *Geophys. Res. Lett.*, *38*, L09602, doi:10.1029/2011GL047174.

Stiver, W., and D. Mackay (1984), Evaporation rate of spills of hydrocarbons and petroleum mixtures, *Environ. Sci. Technol.*, *18*, 834–840, doi:10.1021/es00129a006.

Stiver, W., W. Y. Shiu, and D. Mackay (1988), Evaporation times and ratesof specific hydrocarbons in oil spill, *Environ. Sci. Technol.*, *23*, 101–105, doi:10.1021/es00178a013.

The Federal Interagency Solutions Group, Oil Budget Calculator Science and Engineering Team (2013), *Oil Budget Calculator-Deepwater Horizon*. [Available at http://www.restorethegulf.gov/sites/default/files/documents/pdf/OilBudgetCalc_Full_HQ-Print_111110.pdf.]

Tkacik, D. S., A. A. Presto, N. M. Donahue, and A. L. Robinson (2012), Secondary organic aerosol formation from intermediate-volatility organic compounds: Cyclic, linear, and branched alkanes, *Environ. Sci. Technol.*, *46*, 8773–8781, doi:10.1021/es301112c.

Valentine, D. L., G. B. Fisher, S. C. Bagby, R. K. Nelson, C. M. Reddy, S. P. Sylva, and M. A. Woo (2014), Fallout plume of submerged oil from Deepwater Horizon, *Proc. Natl. Acad. Sci. U. S. A.*, *111*(45), 15,906–15,911, doi:10.1073/pnas.1414873111.

Worton, D. R., H. Zhang, G. Isaacman-VanWertz, A. W. H. Chan, K. R. Wilson, and A. H. Goldstein (2015), Comprehensive chemical characterization of hydrocarbons in NIST standard reference material 2779 Gulf of Mexico crude oil, *Environ. Sci. Technol.*, doi:10.1021/acs.est.5b03472.

Yuan, B., C. Warneke, M. Shao, and J. A. de Gouw (2014), Interpretation of volatile organic compound measurements by proton-transfer-reaction mass spectrometry over the deepwater horizon oil spill, *Int. J. Mass Spectrom.*, *358*, 43–48, doi:10.1016/j.ijms.2013.11.006.